Article

Comprehensive Study of the Effects of Nanopore Structures on Enzyme Activity for the Enzyme Based Electrochemical Biosensors Based on Molecular Simulation

Guang Yang, Bo Liang, Qin Zhu, Yichuan Hu, and Xuesong Ye

J. Phys. Chem. A, **Just Accepted Manuscript** • DOI: 10.1021/acs.jpca.6b10206 • Publication Date (Web): 29 Nov 2016

Comprehensive Study of the Effects of Nanopore Structures on Enzyme Activity for the Enzyme Based Electrochemical Biosensors Based on Molecular Simulation

Guang Yang[a,1], Bo Liang[a,1], Qin Zhu[a], Yichuan Hu[a], Xuesong Ye[a,b,c]*

[a] *Biosensor National Special Laboratory, College of Biomedical Engineering and Instrument Science, Zhejiang University,*
[b] *Cyrus Tang Center for Sensor Materials and Applications, Zhejiang University,*
[c] *State Key Laboratory of CAD & CG, Zhejiang University,*
Hangzhou 310027, PR China

[*] *Corresponding author: Xuesong Ye*
E-mail address: yexuesong@zju.edu.cn

[1] *These authors contributed equally to this work.*

Abstract

Assembly of biocompatible nanostructures to retain the enzyme activity and improve the biocatalytic ability is a decisive factor for enhancing the performance of enzyme biosensors. However, there is still a lack of molecular level understandings of the physicochemical interaction mechanism at the interface of biosensor electrodes and enzymes. Here, for the first time at molecular level, the effects of two classic biosensor electrode materials with different electrical properties and morphologies, and glucose oxidase (GOD) on retaining the enzyme conformation were analyzed by molecular dynamics simulation. First, for the immobilization of GOD, the interfaces of zinc oxide (ZnO) with different electrical properties and 10 nm diameter ZnO nanopore were studied; Then, to simulate the sensing process when electric voltages are applied, positively charged gold planes and 10 nm diameter gold nanopore were investigated as well. The results showed that the nanopore structure was confirmed to be well adapted for the enzyme conformation retaining compared to the plane structure for both ZnO and gold materials, and they almost fit well with the sensitivity measurement results from many previously reported experimental studies. This study also indicates that molecular modeling of the interactions between biomolecules and functional nanostructures is helpful for developing high performance enzyme nanobiosensors.

1. Introduction

Enzymes are highly efficient and specific biocatalyst organisms produced by living cells, playing an irreplaceable important role in life activities. Enzyme

biosensors, using enzymes as molecular recognition elements, have the advantages of good selectivity, high sensitivity, fast response and so on. Since Clark and Lyons proposed the first enzyme biosensor in 1962,[1] with the rapid development of biology, chemistry, medicine, physics, microelectronics technology and other related disciplines, enzyme biosensors have become one of the most active research topics in the areas of biochemical sensors. For example, the enzyme glucose biosensors have been widely studied and benefited hundreds of millions of diabetics all over the world.

In the past decades, many researchers focused on improving the sensitivity and stability performance of enzyme biosensors. Especially in recent years, with the development of nanotechnology, scientists have attempted to use various nanomaterials such as carbon nanotubes,[2-6] graphene,[7-11] metal nanoparticles,[12-14] nanowires [15-17] and their complex [18-20] to build or modify electrodes for improving the performance of enzyme biosensors for their high specific surface area, exceptional electrical properties and so on. However, the difficulties of improving the sensitivity of enzyme biosensors should be discussed with two different concepts which are enzyme immobilization and retaining the activity of immobilized enzymes. Enzyme loss during the immobilization on electrode surface results in a significantly reduced enzyme loading, leading to the decrease of biosensors' sensitivity;[21, 22] At the same time, a lot of experimental results showed that when being utilized in biosensing, most of enzymes lost the activity when immobilized onto nanomaterials while only a part of enzymes played a role in biosensors.[23-27] All in all, in the studies of enzyme

activity on the electrode surfaces, the general view is that the conformation and orientation of adsorbed enzymes at the electrode interface will significantly affect the performance of biosensors because the enzymes are unstable on the electrode surface.[28-30]

Hence, how to construct the biocompatible nanospace for retaining enzyme activity and enhancing its biocatalytic ability is one decisive factor in improving the sensitivity of enzyme biosensors. From an experimental point of view, in the past years, many researchers have studied the effects of different materials based functional nanostructures on the performance of enzyme biosensors, and came to a conclusion that nanopore structures were more suitable for enzyme biosensors.[31-33] What's more, under the same fabrication conditions, studies of enzyme biosensors with nanopore structures having higher sensitivity compared to similar sensors with plane structures have been reported. For classic semiconductive biosensor materials such as ZnO, many research groups reported that ZnO nanopore based biosensors showed higher sensitivities compared to those based on flat ZnO nanorod structure.[34-38] Meanwhile, for conductive metal materials like gold, many researchers increased the sensitivity about 30 times or more higher than flat electrodes by preparing gold nanoporous electrodes modified with biocatalysts.[39-42] However, previous researches discussed the experimental phenomenon using only the experimental results, and there is still a lack of molecular level understandings of the effects of the interactions between biomolecules and nanostructures on enzyme biosensors. What's more, respective experimental investigations by adjusting

experimental conditions to explore the optimized preparation process cannot provide an efficient theoretical guidance for nanobiosensor design.

Molecular dynamics simulation has been successfully applied in many areas such as biological physics,[43, 44] biological chemistry [45, 46] and physical chemistry [47, 48] in recent years. In our previous study, we evaluated the effects of differently charged single-walled carbon nanotubes on the conformation and orientation of glucose oxidase coenzyme FAD using molecular dynamics simulation.[49] With the experimental fact that the sensitivities of nanoporous ZnO based biosensors are higher than that of plane ZnO nanostructure based biosensors, there is a guess of the enzyme denature mechanism during the enzyme immobilization of plane ZnO biosensors based on the statement that the surface chemistry of a nanostructure provides control over the function of adsorbed proteins.[50] And the distribution of the polar atoms strongly affected the conformation of the enzyme and led to its inactivation. According to the speculation mentioned above, different morphology of the gold substrates should not affect the activity of the enzyme while associated with non-polar gold. However, the fact that gold based nanoporous biosensors had higher sensitivity than plane ones were reported in many experimental results as well. Hence, the inactivation of enzymes in gold nanostructure based biosensors may happen in the sensing process when electric voltages were applied. Therefore, manually charged gold substrates with different morphology were studied to simulate the gold electrodes when electric voltages were applied.

Here, taking into consideration that two materials, namely semiconductive ZnO

and metal gold, have been widely used as typical substrates for the development of different biosensors due to the advantages of nontoxicity, biological compatibility, fast electron transfer rates and easy preparation,[51] a set of comprehensive computing models of GOD/ZnO and GOD/gold hybrid systems were generated at molecular level for the first time according to the construction of ZnO based and gold based glucose biosensors by means of general enzyme immobilization processes reported previously[38, 52-54]. At both interfaces of GOD/ZnO and GOD/gold systems, the effects of ZnO and gold planes, 10 nm diameter ZnO and gold nanopores (gold substrates were manually charged to simulate the working condition of biosensors when voltages are applied) on the enzyme conformation were analyzed in details. This study will help to understand the relationships among the enzyme activity, nanostructures and biosensor sensitivity in theoretical calculations.

2. Experimental

GOD is a homodimer with a molecular weight of 160 k Dalton (the length is about 7 nm), and the x-ray structure of GOD was derived from the protein data bank (ID code 1GPE).[55] And in this study, all MD simulations were performed by NAMD [56] program with the force field CHARMM27,[57] utilizing atomic partial charge values of 1.026 e and -1.026 e for Zn and O atoms respectively[58, 59] and 0.08 e for Au atoms to simulate the sensing environment when voltages are applied on gold electrodes. The force field parameters for ZnO and gold were used based on initial computations by Raymand [59] and Heinz [60] respectively. The parameters for the Lennard-Jones potential for the cross interactions between non-bonded atoms were obtained from the

Lorentz-Berthelot combining rule. The GOD enzyme was selected to explore the dynamics behaviors when GOD associated zinc oxide and gold bulks with or without nanopores.

Cylinder wurtzite-type ZnO bulks (with the lattice constants a = 3.25 Å and c = 5.2 Å [61]) with and without sphere nanopores, and cylinder gold bulks (with the lattice constant 4.078 Å [62]) with and without sphere nanopores were generated. First, for the nanostructure size selection, 10 nm diameter half-sphere pores were applied for the ZnO and gold nanopore structures. Second, for the initial orientation selection, two different GOD initial orientations were created. GOD was solvated in a water box and underwent a 1000 steps energy minimization. Then a MD run of the energy minimized system was carried out for 1 ns until the root mean squared deviation and the system total energy fluctuated around a constant value, which indicated that the equilibrium state of GOD was reached. And the final orientation of the equilibrated GOD was chosen as the initial orientation of GOD/ZnO and GOD/gold hybrid systems MD simulations and was denoted as 1-original. And 2-x [90°] was obtained through rotating the 1-original protein prism clockwise around the x-axis by 90°. Third, for the ZnO and gold plane surfaces selection, the positively charged Zn-terminated surfaces (0001) and negatively charged O-terminated surfaces (000 $\bar{1}$) of ZnO planes, and (111) surfaces of gold planes were applied. 1-original and 2-x [90°] GOD were placed above the (0001) surfaces and (000 $\bar{1}$) surfaces of ZnO planes and (111) surfaces of gold planes, as well as inside the 10 nm diameter ZnO and gold nanopores. After that, we solvated the hybrid systems in a TIP3 water box of

size of 169.27 × 169.508 × z $Å^3$, where z varied from 84.29 Å to 195.68 Å to fit the different initial orientations of the protein. Then sodiums and chlorines were added to maintain the charge neutrality of these systems. 5,000-step energy minimizations of every hybrid system were performed, and 1 ns or 2 ns (the simulation time for all systems was 1 ns except that the simulation time for 1-original GOD/ZnO nanopore system was 2 ns because the total interaction energy between GOD and ZnO did not fluctuate around a stable value until the simulation time approached 2 ns) MD runs were done. The main goal of the simulations was focused on the dynamic features of GOD and how the different morphologies and electrical properties of ZnO and gold structures affected the conformation of GOD in the MD runs.

All simulations were performed with a time step of 2 fs, and a cut-off was set with a switching function starting at a distance of 10 Å and reaching zero at 12 Å. A particle mesh Ewald (PME) summation was used to calculate the long-range electrostatic interactions, with a cut-off distance of 12 Å for the separation of the direct and reciprocal space. During the MD simulations, the Langevin method was used to ensure a constant temperature of 310 K and a constant pressure of 1 atm. Periodic boundary conditions were applied for all the simulations. Visualization and analysis of the configurations were performed with the VMD [63] packages and the utility packages included in NAMD.

The time-dependent interaction energy $E_{int}(t)$ for the systems in MD simulations is defined by the Equation (1):

$$E_{int}(t) = E_{Sub+GOD}(t) - E_{Sub}(t) - E_{GOD}(t) \quad (1)$$

where E_{int} (t) stands for the total interaction energy between the GOD and the ZnO or gold at time t during the MD simulation, and $E_{Sub+GOD}$ (t), E_{Sub} (t), E_{GOD} (t) is the total potential energy of the ZnO or gold plus GOD, of the ZnO or gold, and of the GOD at time t during the MD simulation, respectively. The van der Waals (vdW) interaction energy and the electrostatic interaction energy were defined similarly to the total interaction energy. This method has been successfully applied to investigate the adsorption and desorption of proteins or macromolecule on the inorganic material surface.[64-67] The data were saved every 2000 steps and derived from the saved frames within these simulations.

3. Results and discussion

All MD simulations results showed that, during the last 500 ps of all simulations, the Root-Mean-Square Deviation (RMSD) of the ten hybrid systems fluctuated around rather stable values as shown in Figure 1A and C, which implied that stable states were achieved for all the systems investigated. However, in the same GOD initial orientations cases, the values of RMSD of GOD that associated with plane substrates were larger than those of GOD that associated with nanopore substrates as shown in Figure 1B and D, leading to a fact that the orientations and conformations of the GODs above plane substrates changed much more than the GODs inside of nanopore substrates. In addition, interestingly, when analyzing GODs with two different initial orientations, the RMSDs of GODs with 2-x [90°] initial orientation were always larger than those of GODs with 1-original initial orientation as shown in Figure 1B and D, meaning that the orientations and conformations of GODs with 2-x

[90°] initial orientation changed more than those of GODs with 1-original initial orientation on those substrates during the simulations.

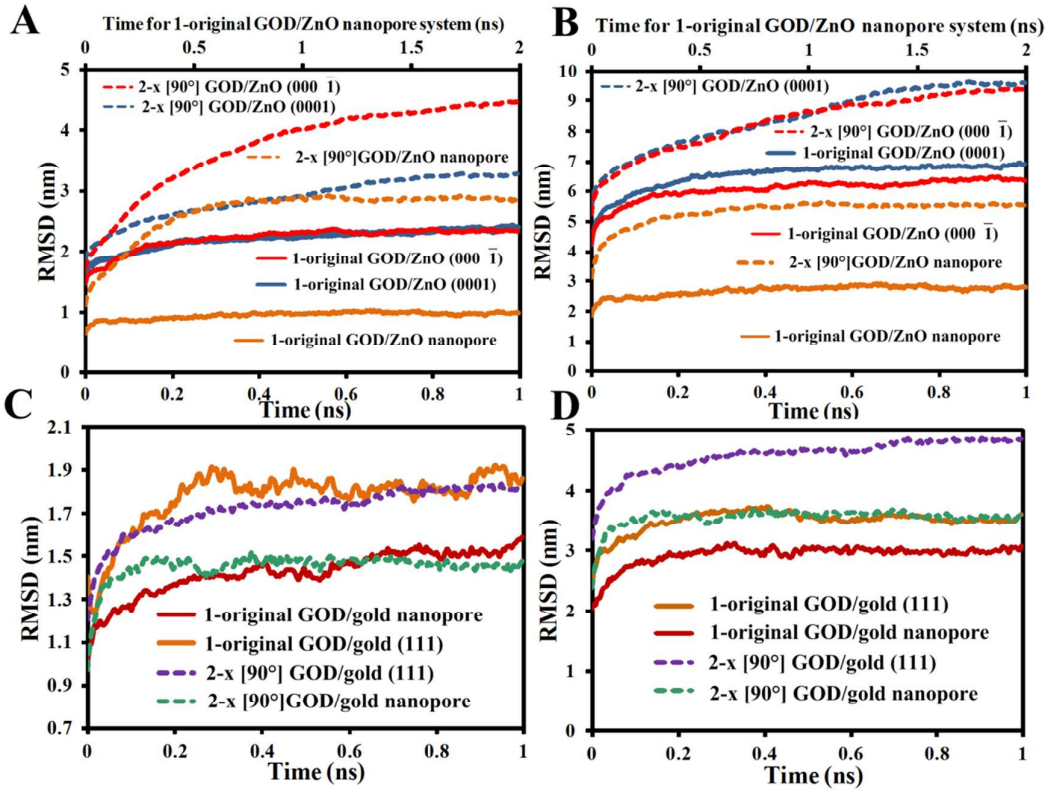

Figure 1. A) RMSDs of six systems that associated with GOD and ZnO substrates, and **B)** RMSDs of six GODs in these six systems that associated with GOD and ZnO substrates, and **C)** RMSDs of four systems that associated with GOD and gold substrates, and **D)** RMSDs of four GODs in these four systems that associated with GOD and gold substrates through these simulations (the simulation time for all ten systems was 1 ns except for 1-original GOD/ZnO nanopore system, which was 2 ns).

3.1 Simulations of the 1-original GOD above the surfaces of differently charged ZnO planes and inside of the 10 nm diameter ZnO nanopore:

The conformation and orientation changes of the 1-original GOD above the ZnO plane surface and inside the 10 nm diameter ZnO nanopore were investigated. The isoelectric point of GOD is 3.8,[68] so in the simulation environment of pH 7.0, GOD is negatively charged. For the (0001) ZnO plane case, the conformation of GOD changed violently as shown in the snapshots in Figure 2A. GOD lost parts of its

secondary structures, which usually leads to enzyme inactivation.[23] The Zn-terminated top layer of the (0001) ZnO plane is polar with strong positive charges, which led to the attraction between ZnO and GOD, and caused GOD to move gently close to ZnO as the normalized center of mass (COM) distance showed in Figure 2B-Right.

In order to quantitatively study the dominant interaction between the ZnO substrate and GOD, the total interaction energy, vdW interaction energy and electrostatic interaction energy between them during the simulation process were calculated. Obvious adsorptions of six amino acids on the ZnO plane were observed by analyzing the trajectory files. Three Glu residues, three Asp residues (the names with certain numbers of all the amino acids in all ten systems were named by the simulation protein data bank files), which are all acidic amino acids with negative charges, adsorbed onto the ZnO surface within 200 ps as the normalized COM distance data showed in Figure 2B-Right, which caused an interaction energy decrease from -8632.03 kJ/mol to -9371.42 kJ/mol as shown in Figure 2B-Left within 200 ps. Then caused by the strong electrostatic attraction between the positively charged ZnO surface and negatively charged GOD, GOD slightly moved towards the surface of plane ZnO substrate as the normalized COM distance showed in Figure 2B-Right with the total interaction energy between GOD and ZnO decreasing to -9576.10 kJ/mol approximately in the end of the MD simulation. With about 97.38 % contribution from electrostatic interaction energy, GOD went through noticeable conformation changes caused by the strong electrostatic interaction at the end of the

simulation, indicating that the electrostatic attraction between the positively charged ZnO and negatively charged GOD was the major reason that caused the orientation and violent conformation changes of GOD.

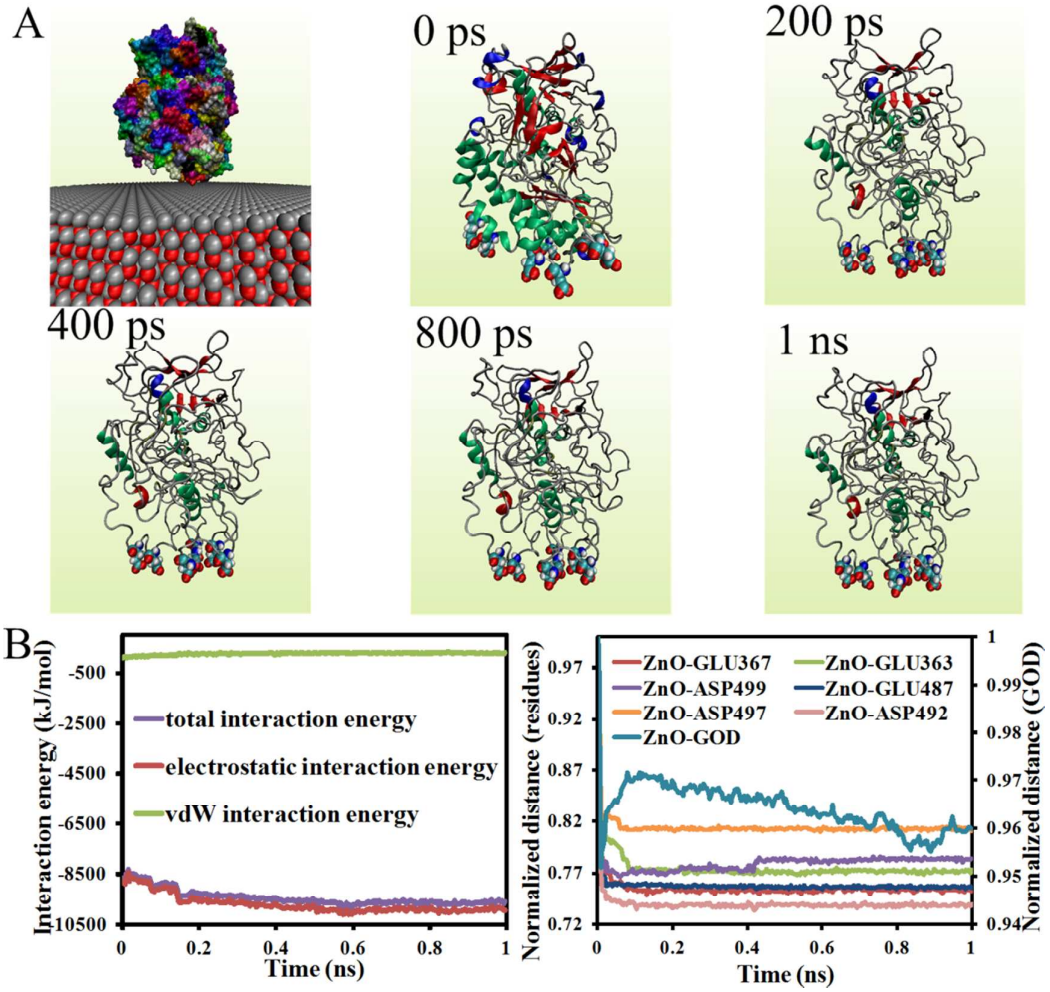

Figure 2. A) Snapshots of the 1-original GOD above the (0001) ZnO plane (the ZnO displayed by vdW model in the first snapshot; the GOD displayed by Surf model in the first snapshot, and NewCartoon model and colored in secondary structure mode in the rest snapshots; the six amino acids displayed in vdW model. Water molecules and counterions are not displayed here for clarity) during the 1 ns simulation. **B) Left:** The total, vdW and electrostatic interaction energies between the 1-original GOD and (0001) ZnO plane. **Right:** The normalized COM distances between the six amino acids, 1-original GOD and (0001) ZnO plane during the 1 ns simulation.

For the (000 $\bar{1}$) ZnO plane case, the conformation of 1-original GOD changed violently and lost many secondary structures within 200 ps as shown in Figure 3A. Six positively charged basic amino acids, which were three Lys residues and three

Arg residues, adsorbed onto the ZnO plane within 200 ps as the normalized COM distance data and the snapshots showed in Figure 3, causing the total interaction energy decreased from -5743.07 kJ/mol to -6095.23 kJ/mol as shown in Figure 3B-Left. In the first 200 ps, caused by the electrostatic repulsion between the negatively charged GOD and O-terminated ZnO surface, GOD moved away from the ZnO surface. However, pulled by the six amino acids, which was caused by strong electrostatic interaction between them and the ZnO surface, GOD moved gently towards the ZnO substrate from 1.021 to 1.005 as the normalized COM distance showed in Figure 3B-Right. 98.12 % contributed by electrostatic interaction energy, the interaction energy between GOD and ZnO fluctuated around -6156.75 kJ/mol till the end of the MD simulation as shown in Figure 3B-Left, indicating that the strong electrostatic interaction between all O atoms of the ZnO top layer and GOD was the major reason that caused the orientation and conformation changes of GOD.

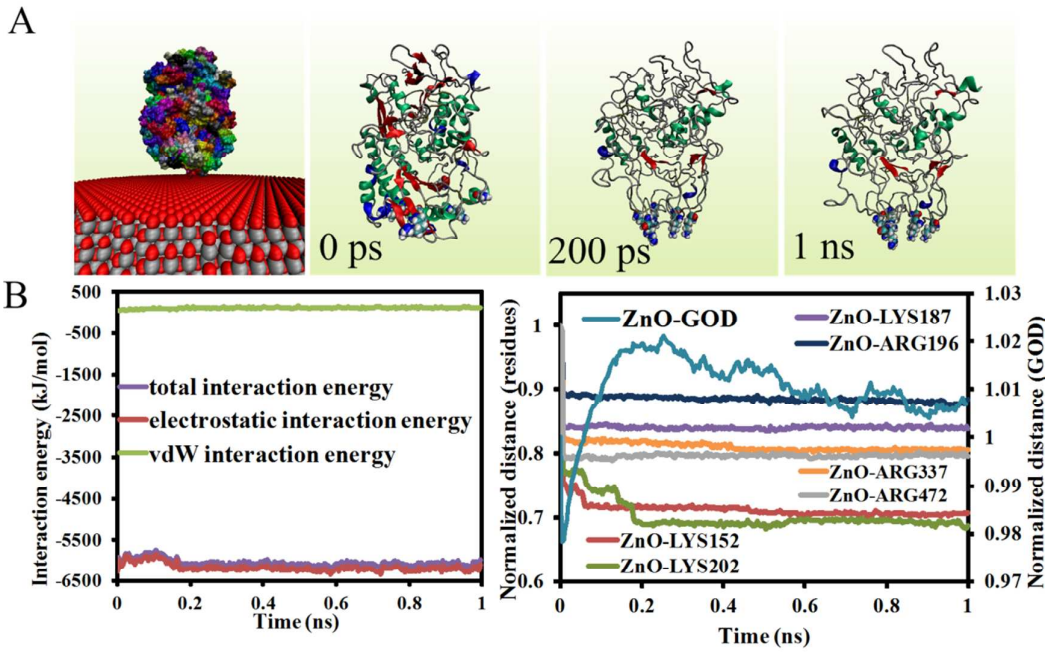

Figure 3. A) Snapshots of the 1-original GOD above the (000 $\bar{1}$) ZnO plane (the ZnO displayed by vdW model in the first snapshot; the GOD displayed by Surf model in the first snapshot, and NewCartoon model and colored in secondary structure mode in the rest snapshots; the six amino acids displayed in vdW model. Water molecules and counterions are not displayed here for clarity) during the 1 ns simulation. **B) Left:** The total, vdW and electrostatic interaction energies between the 1-original GOD and (000 $\bar{1}$) ZnO plane. **Right:** The normalized COM distances between the six amino acids, 1-original GOD and (000 $\bar{1}$) ZnO plane during the 1 ns simulation.

For the ZnO substrate with 10 nm diameter pore, there was very little conformation change of the 1-original GOD and its whole secondary structure stayed almost the same as the snapshots shown in Figure 4A, which brought possibility for an active enzyme. The 1-original GOD moved slightly towards ZnO within 300 ps and the normalized COM distance fluctuated around 0.84 till the end of the simulation as shown in Figure 4B. The total and electrostatic interaction energy fluctuated around 6.39 kJ/mol as showed in Figure 4B. As analyzed above, the 10 nm diameter ZnO pore least affected the conformation of 1-original GOD compared with both (0001) and (000 $\bar{1}$) ZnO plane surfaces.

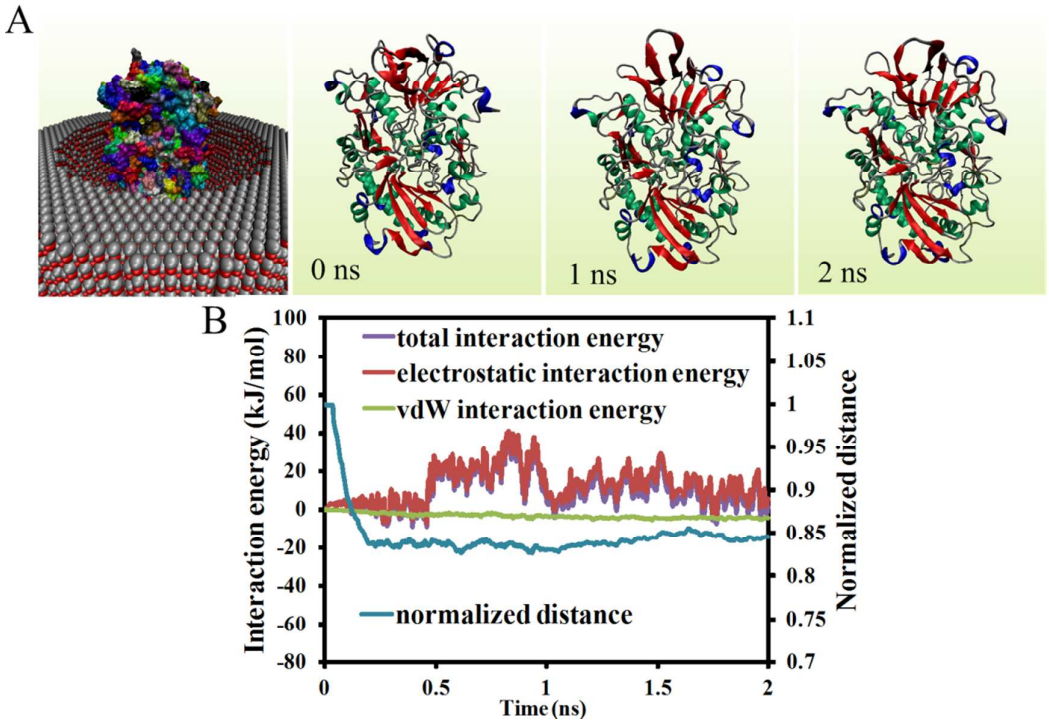

Figure 4. A) Snapshots of the 1-original GOD inside the 10 nm diameter ZnO nanopore (the ZnO displayed by vdW model in the first snapshot; the GOD displayed by Surf model in the first snapshot, and NewCartoon model and colored in secondary structure mode in the rest snapshots. Water molecules and counterions are not displayed here for clarity) during the 2 ns simulation. **B)** The total, vdW and electrostatic interaction energies between the 1-original GOD and 10 nm diameter ZnO nanopore, and the normalized COM distances between 1-original GOD and 10 nm diameter ZnO nanopore during the 2 ns simulation.

3.2 Simulations of the 2-x [90°] GOD above the surfaces of differently charged ZnO planes and inside of the 10 nm diameter ZnO nanopore:

2-x [90°] GOD and ZnO hybrid systems were generated as comparisons to investigate how differently the conformation and orientation might change with different initial orientations of GOD. For the (0001) ZnO surface case, caused by the strong electrostatic interaction, ten Asp residues and eight Glu residues (two of each were chosen to be analyzed), which are all negatively charged acidic amino acids, adsorbed onto the surface of the ZnO plane of which its top layer is made of positively charged Zn atoms within 200 ps, causing the first mild total interaction energy drop from -20086.82 kJ/mol to -22010.11 kJ/mol as shown in the snapshots in Figure 5A and the interaction energy data in Figure 5B-Left. As the simulation went on, driven by the strong electrostatic repulsion between the positively charged basic amino acids and Zn-terminated ZnO surface, two Lys residues and two Arg residues started to move away from the ZnO substrate after 200 ps. The electrostatic repulsion was so strong that it made the basic amino acids moved even further away from the ZnO suface around about 700 ps, causing another total interaction energy drop from -23050.23 kJ/mol to -24016.79 kJ/mol as shown in Figure 5B-Left. The violent movement of these four basic amino acids till the end of the simulation pulled the GOD away from the ZnO surface as the normalized COM distance data showed in

Figure 5B-Right. The electrostatic attraction between the acidic amino acids and the ZnO surface, and the electrostatic repulsion between the basic amino acids and the ZnO surface fought against with each other violently and pulled the GOD towards two different directions, leading to the enormous conformation changes of the GOD and the loss of almost all of its secondary structures which could lead to enzyme inactivation as the snapshots shown in Figure 5A. The total interaction energy between GOD and ZnO, 97.67% of which was contributed by electrostatic interaction energy, went through a drop from -19799.11 kJ/mol to -24284.71 kJ/mol approximately as shown in Figure 5B-Left, indicating that electrostatic attraction was the main reason which caused the denaturation of the enzyme.

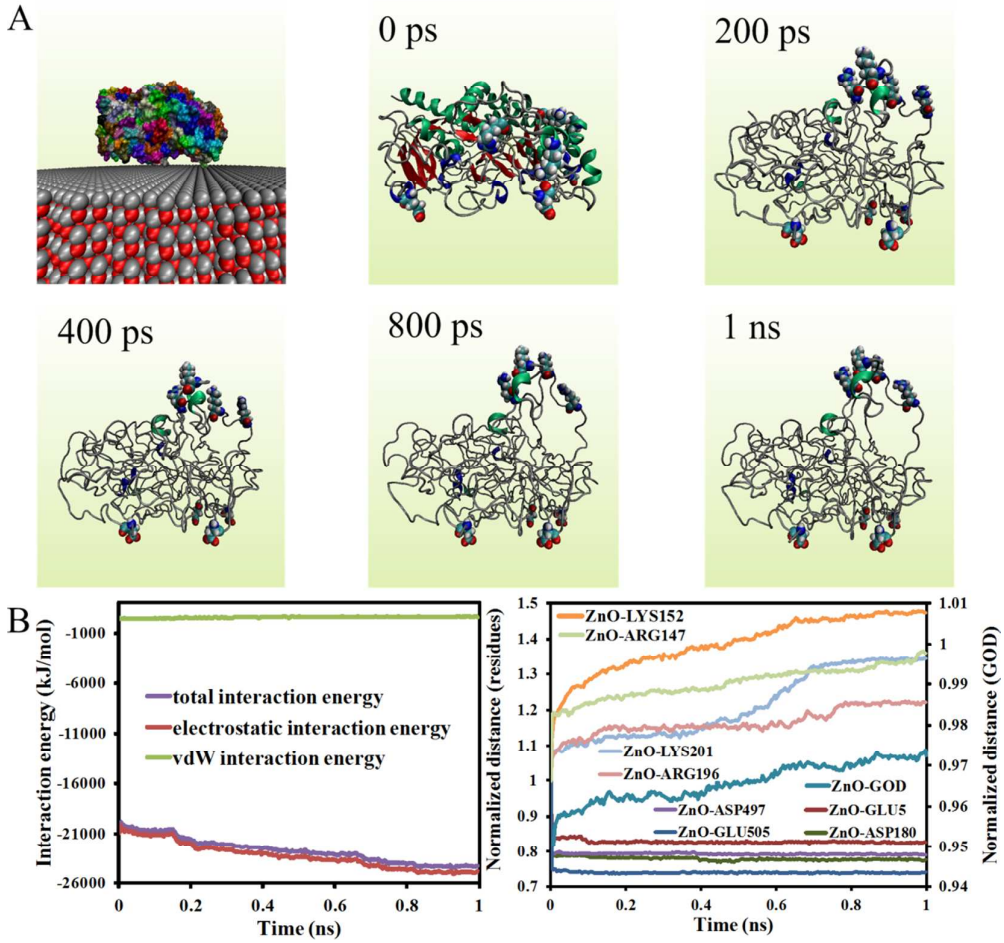

Figure 5. A) Snapshots of the 2-x [90°] GOD above the (0001) ZnO plane (the ZnO displayed by vdW model in the first snapshot; the GOD displayed by Surf model in the first snapshot, and NewCartoon model and colored in secondary structure mode in the rest snapshots; the eight amino acids displayed in vdW model. Water molecules and counterions are not displayed here for clarity) during the 1 ns simulation. **B) Left:** The total, vdW and electrostatic interaction energies between the 2-x [90°] GOD and (0001) ZnO plane. **Right:** The normalized COM distances between the eight amino acids, 2-x [90°] GOD and (0001) ZnO plane during the 1 ns simulation.

For the $(000\ \bar{1})$ ZnO plane case, three Arg residues and one Lys residue, which are positively charged basic amino acids, adsorbed onto the negatively charged O-terminated polar surface of ZnO within 100 ps, which caused an obvious total interaction energy drop from -6581.92 kJ/mol to -7644.01 kJ/mol as the data shown in Figure 6B-Left. Meanwhile, as the simulation went on, caused by the repulsion of the same electrical property, negatively charged GOD had the tendency to move away from the surface of ZnO. The electrostatic repulsion drove GOD to move away from the ZnO surface, causing the total interaction energy to decrease to -11660.54 kJ/mol around about 600 ps as shown in Figure 6B-Left. As the simulation went on, the strong electrostatic adsorption of the six basic amino acids still existed, leading to the enormous conformational changes of the GOD till the end of the simulation. In addition, GOD lost most of its secondary structures, as the snapshots shown in Figure 6A, which could lead to enzyme inactivation. GOD moved slightly away from ZnO substrate as the normalized COM distance between them increased from 0.97 to 1.18 as shown in Figure 6B-Right, and the total interaction energy between 2-x [90°] GOD and ZnO, which was contributed 98.48% by the electrostatic interaction energy, went through a drop from -8014.13 kJ/mol to -12013.52 kJ/mol through the whole simulation as shown in Figure 6B-Left, indicating that the electrostatic interaction played a key role in the deformation of the GOD.

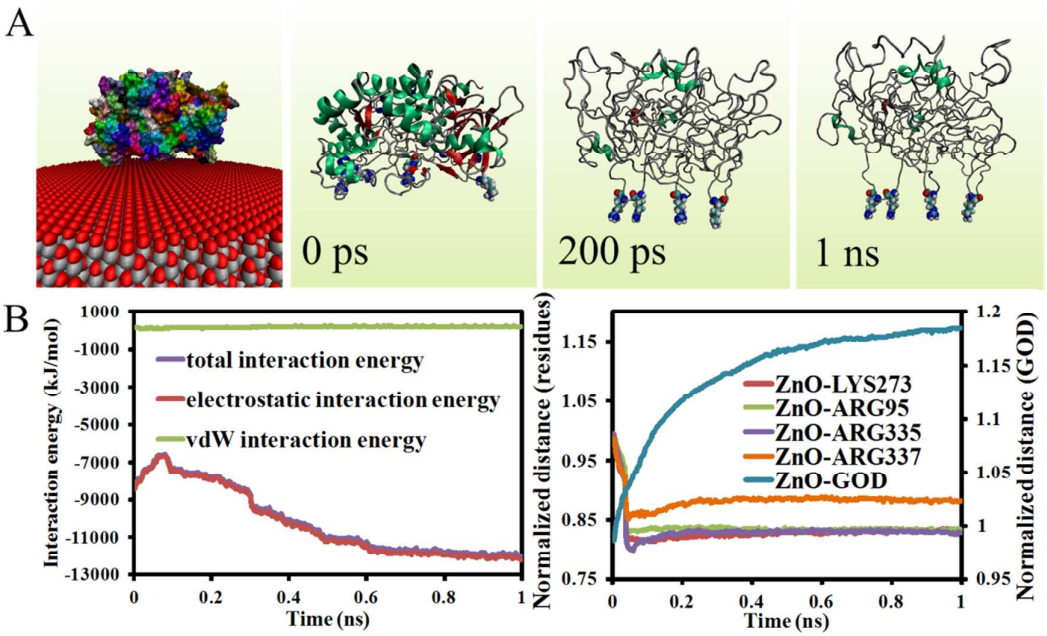

Figure 6. A) Snapshots of the 2-x [90°] GOD above the (000 $\bar{1}$) ZnO plane (the ZnO displayed by vdW model in the first snapshot; the GOD displayed by Surf model in the first snapshot, and NewCartoon model and colored in secondary structure mode in the rest snapshots; the four amino acids displayed in vdW model. Water molecules and counterions are not displayed here for clarity) during the 1 ns simulation. **B) Left:** The total, vdW and electrostatic interaction energies between the 2-x [90°] GOD and (000 $\bar{1}$) ZnO plane. **Right:** The normalized COM distances between the four amino acids, 2-x [90°] GOD and (000 $\bar{1}$) ZnO plane during the 1 ns simulation.

Inside of the 10 nm diameter ZnO nanopore substrate, the 2-x [90°] GOD moved slightly towards ZnO as the normalized COM distance between GOD and ZnO decreased from 0.983 to 0.728 as shown in Figure 7B. With an 89.98% contribution of the electrostatic interaction energy, the total interaction energy dropped from about -209.95 kJ/mol to -1045.39 kJ/mol at the end of the 1 ns simulation as shown in Figure 7B. Little conformation change of the GOD was observed and most of its secondary structures stayed the same during the simulation as the snapshots showed in Figure 7A, which was similar to the 1-original GOD inside the 10 nm diameter ZnO pore described above.

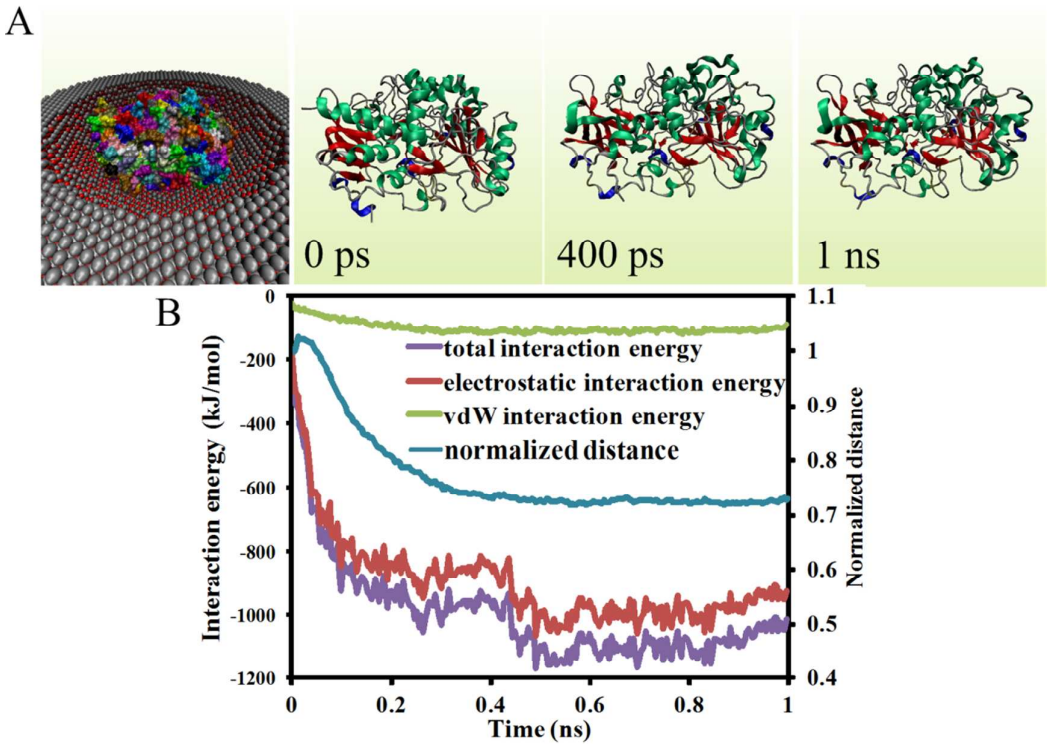

Figure 7. A) Snapshots of the 2-x [90°] GOD inside the 10 nm diameter ZnO nanopore (the ZnO displayed by vdW model in the first snapshot; the GOD displayed by Surf model in the first snapshot, and NewCartoon model and colored in secondary structure mode in the rest snapshots. Water molecules and counterions are not displayed here for clarity) during the 1 ns simulation. **B)** The total, vdW and electrostatic interaction energies between the 2-x [90°] GOD and 10 nm diameter ZnO nanopore, and the normalized COM distances between 2-x [90°] GOD and 10 nm diameter ZnO nanopore during the 1 ns simulation.

As the electrostatic interaction was the dominant part in GOD adsorbing onto the ZnO plane surface, as analyzed above, the effect of the polar surface on GOD adsorption was considered to be of great importance. Compared with the ZnO plane, the 10 nm diameter ZnO nanopore seemed to bring much less electrostatic interactions to GOD and conformation and orientation changes of GOD.

3.3 Simulations of the 1-original GOD above the surface of positively charged gold plane and inside of the 10 nm diameter gold nanopore:

As widely as it has been utilized in biosensors in the past decades, gold was studied as a conductor electrode material in this research as well. For 1-original GOD

above the gold plane surface, Asp195, Asp497 and Glu194, which were all negatively charged acidic amino acids adsorbed onto the gold surface within 50 ps, causing the total interaction energy to go through a drop from -257.69 kJ/mol to -431.88 kJ/mol, and then decreased to -503.73 kJ/mol till around 200 ps as shown in Figure 8B-Left while the other three acidic amino acids moving closer to the gold substrate as the normalized COM distances shown in Figure 8B-Right. And driven by the electrostatic attraction between the positively charged gold plane substrate and the negatively charged acidic amino acids as well, Glu363, Asp499 adsorbed onto the gold surface right after 200 ps along with Asp360 adsorbing onto the gold surface around 400 ps as the normalized COM distance data showed in Figure 8B-Right, which caused the total interaction energy to decrease to -612.04 kJ/mol around 400 ps and fluctuated around -632.62 kJ/mol till the end of the 1 ns MD simulation as shown in Figure 8B-Left. Negatively charged GOD moved gently towards positively charged gold plane surface as the normalized COM distance reduced from 0.992 to 0.971 as shown in Figure 8B-Right, due to the electrostatic interaction energy between them as a 97.08% contribution to the total interaction energy. As the attraction went on, GOD lost some of its secondary structures at the end of the simulation as the snapshots shown in Figure 8A and might lead to its inactivation.

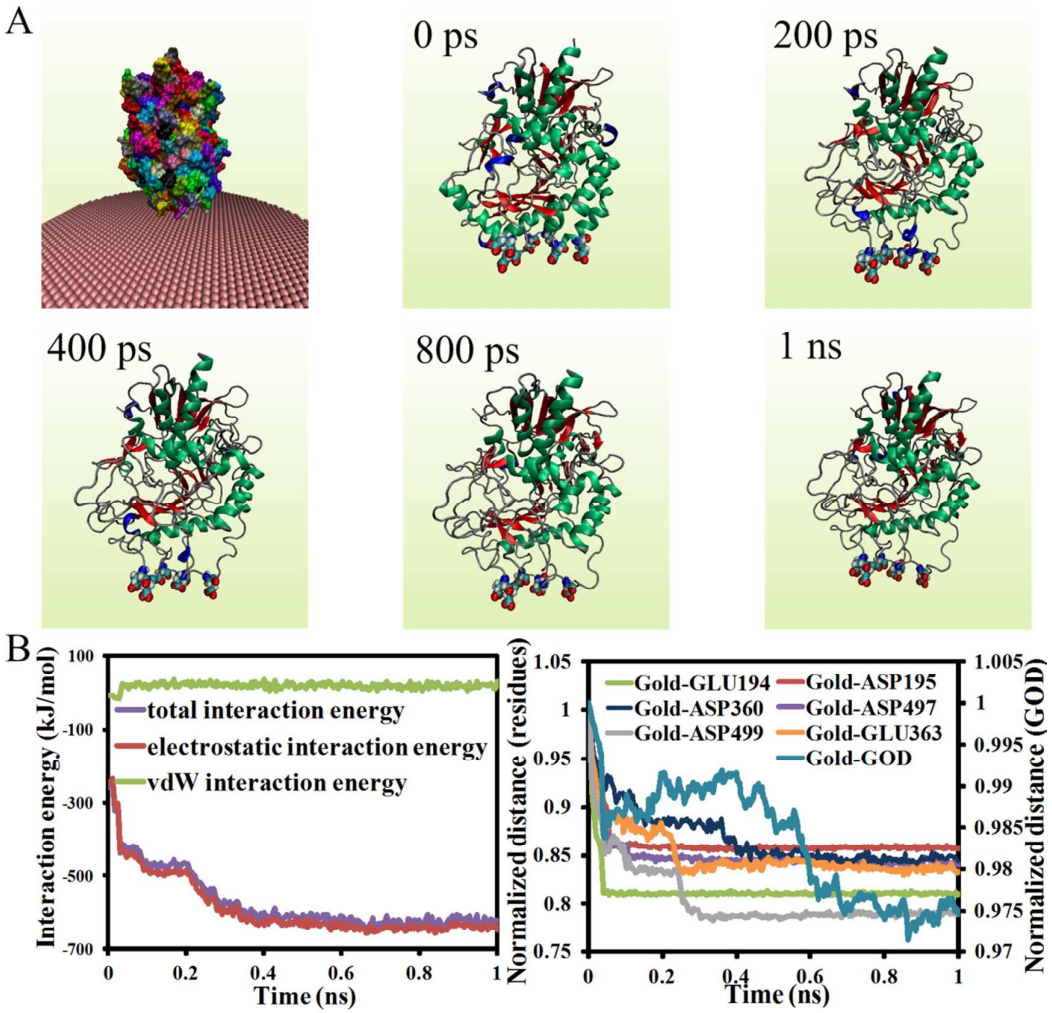

Figure 8. A) Snapshots of the 1-original GOD above the (111) gold plane (the gold displayed by vdW model in the first snapshot; the GOD displayed by Surf model in the first snapshot, and NewCartoon model and colored in secondary structure mode in the rest snapshots; the six amino acids displayed in vdW model. Water molecules and counterions are not displayed here for clarity) during the 1 ns simulation. **B) Left:** The total, vdW and electrostatic interaction energies between the 1-original GOD and (111) gold plane. **Right:** The normalized COM distances between the six amino acids, 1-original GOD and (111) gold plane during the 1 ns simulation.

For 1-original GOD inside of the 10 nm diameter gold nanopore case, there was little conformational change of GOD inside the 10 nm diameter gold nanopore and most of its secondary structure stayed the same as the snapshots shown in Figure 9A during the whole simulation. This half sphere shaped gold nanopore effected the conformation of GOD much less than the plane gold substrate. The GOD moved slightly away from the gold nanopore as the normalized COM distance fluctuated

around 0.94 and the total interaction energies, 90.95% contributed by electrostatic interaction energy, fluctuated very mildly around -2147.16 kJ/mol at the end of the simulation as shown in Figure 9B. In addition, compared with the gold plane case, the 1-original GOD stayed most of its initial conformation.

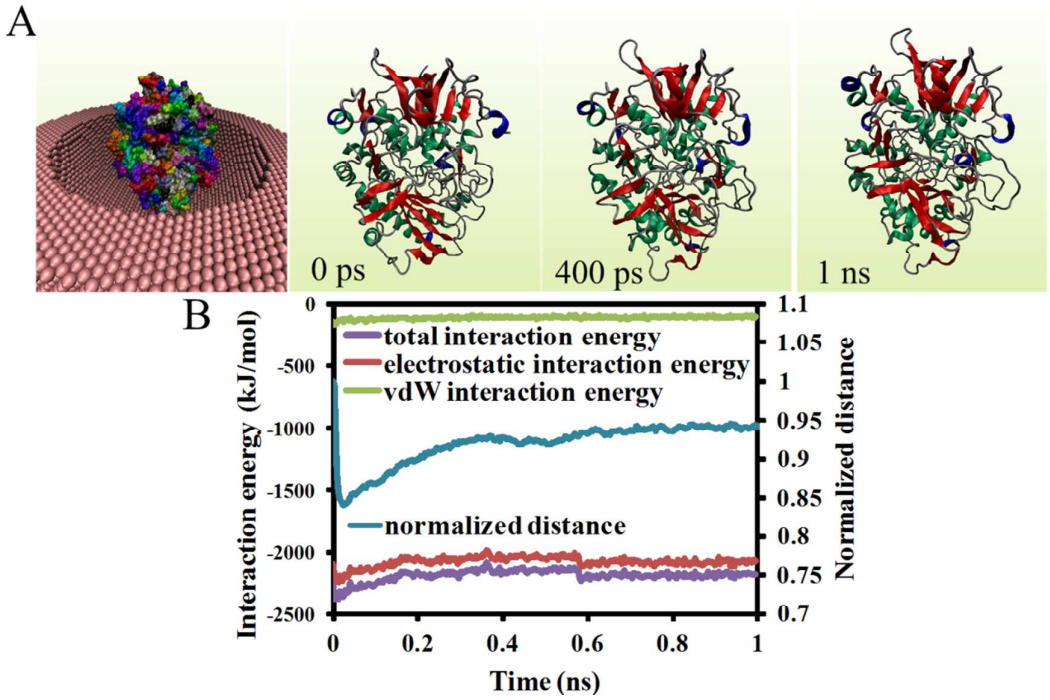

Figure 9. A) Snapshots of the 1-original GOD inside the 10 nm diameter gold nanopore (the gold displayed by vdW model in the first snapshot; the GOD displayed by Surf model in the first snapshot, and NewCartoon model and colored in secondary structure mode in the rest snapshots. Water molecules and counterions are not displayed here for clarity) during the 1 ns simulation. **B)** The total, vdW and electrostatic interaction energies between the 1-original GOD and 10 nm diameter gold nanopore, and the normalized COM distances between 1-original GOD and 10 nm diameter gold nanopore during the 1 ns simulation.

3.4 Simulations of the 2-x [90°] GOD above the surface of differently charged gold plane and inside of the 10 nm diameter gold nanopore:

2-x [90°] GOD and gold hybrid systems were studied as comparisons to investigate how differently the conformation and orientation changed with different initial orientations of GOD. For the gold plane surface case, with the strong

electrostatic interaction between positively charged gold plane substrate and negatively charged acidic amino acids, three Glu residues and three Asp residues adsorbed onto the gold substrate immediately at the beginning of the simulation as the normalized COM data demonstrated in Figure 10B-Right. Caused by Asp499 moving closer to the gold plane surface and Asp11 adsorbing onto the gold surface around 300 ps as the normalized COM distance showed in Figure 10B-Right, which was driven by the electrostatic attraction, the total interaction energy between gold substrate and GOD dropped from -1129.23kJ/mol to -1177.53 kJ/mol as shown in Figure 10B-Left. And Asp499 finally adsorbed onto the gold surface around 700 ps as the normalized COM distance shown in Figure 10B-Right, causing the total interaction energy to decrease from -1188.28 kJ/mol to -1297.89 kJ/mol and fluctuated around -1295.95 kJ/mol till the end of the simulation. It was electrostatic interaction, which contributed 99.47% to the total interaction, that forced the GOD to lose some of its secondary structures and may denature during the whole simulation as the snapshots showed in Figure 10A.

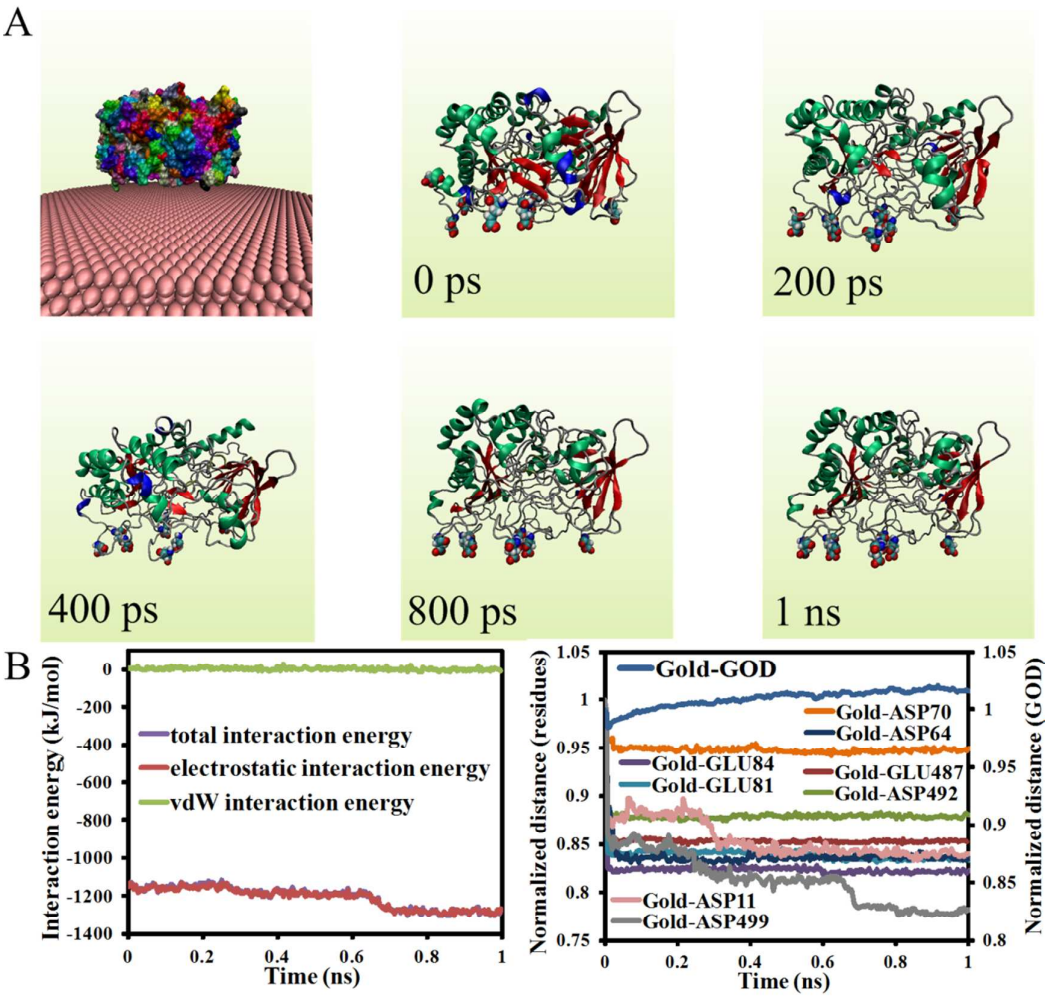

Figure 10. A) Snapshots of the 2-x [90°] GOD above the (111) gold plane (the gold displayed by vdW model in the first snapshot; the GOD displayed by Surf model in the first snapshot, and NewCartoon model and colored in secondary structure mode in the rest snapshots; the eight amino acids displayed in vdW model. Water molecules and counterions are not displayed here for clarity) during the 1 ns simulation. **B) Left:** The total, vdW and electrostatic interaction energies between the 2-x [90°] GOD and (111) gold plane. **Right:** The normalized COM distances between the eight amino acids, 2-x [90°] GOD and (111) gold plane during the 1 ns simulation.

Inside of the 10 nm diameter gold nanopore, the 2-x [90°] GOD moved slightly back and forth as the normalized COM distance fluctuated around 0.87 as shown in Figure 11B. Compared with gold plane substrate, the electrostatic attraction of the half sphere shaped gold nanopore effected the 2-x [90°] GOD much less as the electrostatic interaction energy (which fluctuated around -928.17 kJ/mol as shown in Figure 11B) contribution was 85.90% which was 13.57% less than gold plane case.

Furthermore, there was little conformational change of GOD and GOD maintained most of its secondary structures during the simulation as the snapshots showed in Figure 11A. On top of that, the nanopore structure may keep GOD most of its activity, as to say may keep enzyme biosensors sensitivity when it is associated.

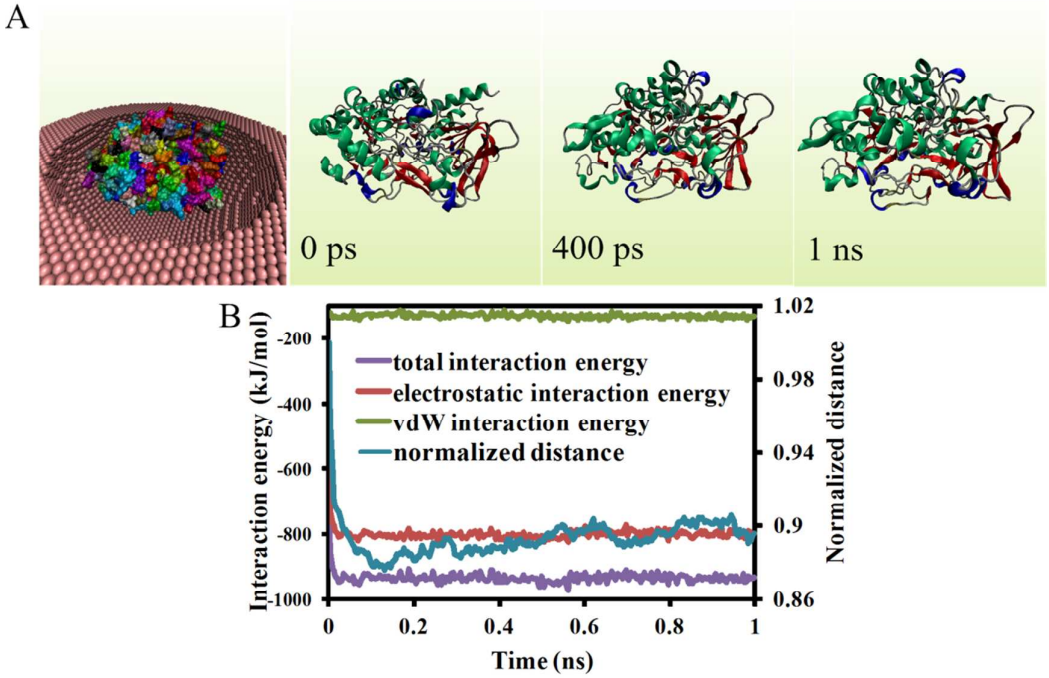

Figure 11. A) Snapshots of the 2-x [90°] GOD inside the 10 nm diameter gold nanopore (the gold displayed by vdW model in the first snapshot; the GOD displayed by Surf model in the first snapshot, and NewCartoon model and colored in secondary structure mode in the rest snapshots. Water molecules and counterions are not displayed here for clarity) during the 1 ns simulation. **B)** The total, vdW and electrostatic interaction energies between the 2-x [90°] GOD and 10 nm diameter gold nanopore, and the normalized COM distances between 2-x [90°] GOD and 10 nm diameter gold nanopore during the 1 ns simulation.

In summary, GOD had a tendency to adsorb onto ZnO and gold plane surfaces due to the electrostatic attractions between certain amino acids and the plane substrates, and went through enormous deformations even lost secondary structures. Meanwhile, the behaviors of GOD were much milder in both ZnO and gold nanopores within the simulations. The total interaction energy, normalized COM distance between GOD and each substrate and RMSDs in the 10 simulation systems are

summarized in Table 1. Furthermore, it is an amazingly interesting fact that different morphologies of nanostructures could cause different conformation changes of GOD. In order to well understand the phenomena why the nanopores could mostly maintain the conformation of GOD enzymes, the charge distributions on the surface of nanopores were further discussed as follows.

When observing the charge distribution on the surface of ZnO nanopores, both the positive charges of Zn atoms and negative charges of O atoms were alternately and evenly distributed inside the pores, causing the whole sphere surface charges closely equaled to neutral when accumulating all charges along with axial direction. Hence, it implied that the electrostatic attractions between every site of the nanopore surfaces and GOD molecules were well balanced, leading to little change of GOD conformation within the 1 ns simulation, which brought better immobilizations when associated with ZnO nanopore structure biosensors [53, 69] where the sensitivity on ZnO planes was 7 μA/(mM cm^2) while 65.82 μA/(mM cm^2) on 80 nm diameter ZnO nanopores. In addition, it was also reported that the secondary structure and bioactivity of GOD molecules could be well reserved when immobilized on the ZnO nanopores.[53, 69] Specifically for GOD-functionalized ZnO substrates, the nanoporous ZnO electrode, which was built by Xia's group using PMMA as a template, brought better GOD immobilization and enhanced the sensitivity 18 times higher than plane ZnO electrode towards the detection of glucose.[70] The glucose biosensor built by Zhou's group based on nanoporous ZnO films exhibited good high sensitivity with good stability and biocompatibility.[71] The unique morphology of nanoporous ZnO

substrate, reported by Fatemi's group, brought better GOD immobilization and higher sensitivity towards glucose than plane ZnO substrate in glucose biosensors.[72] Meanwhile, positively charged gold nanostructures were studied as well to simulate the working situation of biosensors when electric voltages were applied. Compared with the gold planes, the electrostatic attraction influence became much smaller with 10 nm diameter gold nanopores while the electric distribution was much more even alone the curvature of the sphere surfaces and the electrostatic attraction came from every direction instead of one direction with gold planes. In fact, in the experimental researches of GOD/gold glucose biosensors, the sensitivity of the gold nanopore based biosensors was higher than that of the gold plane based biosensors.[73] Nanoporous gold, as an excellent conductor, based biosensor greatly enhanced electrocatalysis compared with the gold plane electrode for the detection of glucose in Kashefi group's research.[74] Compared with plane gold sheet electrode, GOD modified nanopore gold based biosensor, which constructed by Qiu's group, exhibited wider linear range, lower detection limit and higher sensitivity towards glucose.[75] Chen's group reported an GOD modified nanoporous gold biosensor with excellent selectivity and higher sensitivity than plane structure biosensors towards the detection of glucose because of the effective immobilization and excellent electron transfer between the enzyme and the nanoporous gold substrates.[76] Made by Wu's group dealloying 12-carat white gold leaves, GOD functionalized gold nanopore biosensor possessed a larger linear range, lower detection limit, and higher sensitivity than plane

structure based biosensor in glucose biosensing.[52] The change tendency of the sensitivity of these experiments confirmed the above simulation results.

Table 1. The total interaction energy and normalized COM distance between GOD and each substrates, and RMSDs of each system and GOD in these 10 simulation systems

The total interaction energy between GOD and each substrates in the 10 simulation systems				
simulation systems	$E_{0\ ps}$ (kJ/mol)	$E_{400\ ps}$ (kJ/mol)	$E_{800\ ps}$ (kJ/mol)	$E_{1000\ ps}$ (kJ/mol)
1-original GOD above (0001) ZnO plane	-8322.42	-9455.46	-9575.71	-9680.05
1-original GOD above (000 $\bar{1}$) ZnO plane	-5820.03	-6048.22	-6087.54	-6119.22
2-x [90°] GOD above (0001) ZnO plane	-20349.30	-22435.41	-24167.43	-24356.67
2-x [90°] GOD above (000 $\bar{1}$) ZnO plane	-7866.37	-10074.53	-11792.13	-12013.52
2-x [90°] GOD inside of ZnO nanopore	-312.64	-959.19	-1085.89	-1045.39
1-original GOD above (111) gold plane	-257.96	-609.83	-634.71	-636.89
1-original GOD inside of gold nanopore	-2250.24	-2173.53	-2188.68	-2180.56
2-x [90°] GOD above (111) gold plane	-1128.94	-1167.01	-1269.35	-1292.82
2-x [90°] GOD inside of gold nanopore	-927.54	-937.41	-940.58	-946.99
	$E_{0\ ps}$ (kJ/mol)	$E_{600\ ps}$ (kJ/mol)	$E_{1200\ ps}$ (kJ/mol)	$E_{2000\ ps}$ (kJ/mol)
1-original GOD inside of ZnO nanopore	1.65	12.42	8.55	1.16
The normalized COM distance between GOD and each substrates in the 10 simulation systems				
simulation systems	$D_{0\ ps}$	$D_{400\ ps}$	$D_{800\ ps}$	$D_{1000\ ps}$
1-original GOD above (0001) ZnO plane	1	0.967	0.961	0.959
1-original GOD above (000 $\bar{1}$) ZnO plane	1	1.014	1.009	1.006
2-x [90°] GOD above (0001) ZnO plane	1	0.963	0.969	0.973
2-x [90°] GOD above (000 $\bar{1}$) ZnO plane	1	1.152	1.177	1.184

2-x [90°] GOD inside of ZnO nanopore	1	0.732	0.721	0.731
1-original GOD above (111) gold plane	1	0.991	0.975	0.971
1-original GOD inside of gold nanopore	1	0.928	0.937	0.943
2-x [90°] GOD above (111) gold plane	1	1.009	1.017	1.016
2-x [90°] GOD inside of gold nanopore	1	0.888	0.896	0.895
	$D_{0\ ps}$	$D_{600\ ps}$	$D_{1200\ ps}$	$D_{2000\ ps}$
1-original GOD inside of ZnO nanopore	1	0.828	0.839	0.845

The RMSDs of each system and GOD in the 10 simulation systems

simulation systems	system		GOD	
	$RMSD_{start}$(nm)	$RMSD_{end}$(nm)	$RMSD_{start}$(nm)	$RMSD_{end}$(nm)
1-original GOD above (0001) ZnO plane	1.71	2.39	4.61	6.93
1-original GOD above (000 $\bar{1}$) ZnO plane	1.57	2.33	4.63	6.37
1-original GOD inside of ZnO nanopore	0.69	0.97	1.97	2.75
2-x [90°] GOD above (0001) ZnO plane	1.96	3.28	5.85	9.58
2-x [90°] GOD above (000 $\bar{1}$) ZnO plane	1.83	4.48	5.68	9.40
2-x [90°] GOD inside of ZnO nanopore	1.25	2.84	3.46	5.53
1-original GOD above (111) gold plane	1.31	1.86	2.65	3.61
1-original GOD inside of gold nanopore	1.07	1.58	2.11	3.07
2-x [90°] GOD above (111) gold plane	1.26	1.82	3.37	4.85
2-x [90°] GOD inside of gold nanopore	1.06	1.47	2.61	3.62

$E_{0\ ps}$, $E_{400\ ps}$, $E_{800\ ps}$ and $E_{1000\ ps}$ stands for the total interaction energy between GOD and ZnO or gold at 0 ps, 400 ps, 800 ps, 1000 ps respectively during the 1 ns simulation in each system except 1-original GOD inside of ZnO nanopore system. $E_{0\ ps,}$ $E_{600\ ps,}$ $E_{1200\ ps,}$ $E_{2000\ ps}$ stands for the total interaction energy between 1-original GOD and ZnO nanopore at 0 ps, 600 ps, 1200 ps, 2000 ps respectively during the 2 ns simulation. $D_{0\ ps}$, $D_{400\ ps}$, $D_{800\ ps}$ and $D_{1000\ ps}$ stands for the normalized COM distance between GOD and ZnO or gold at 0 ps, 400 ps, 800 ps, 1000 ps respectively during the 1 ns simulation in each system except 1-original GOD inside of ZnO nanopore system. D_0

$_{ps}$, $D_{600\,ps}$, $D_{1200\,ps}$, $D_{2000\,ps}$ stands for the normalized COM distance between 1-original GOD and ZnO nanopore at 0 ps, 600 ps, 1200 ps, 2000 ps respectively during the 2 ns simulation. $RMSD_{start}$ and $RMSD_{end}$ stands for the RMSD value of the system or GOD when the simulation started and ended respectively in each simulation system.

In these MD simulations, it was found that the different morphology and electric properties of ZnO and gold surfaces had different influences on the behaviors of GOD. GODs had enormous conformation changes above both ZnO and gold planes and lost their secondary structures in varying degrees, which could be one of the crucial reasons to enzyme inactivation or even low sensitivity in plane structure based biosensors cases. On the contrary, the fact that the conformations of GODs inside of both ZnO and gold nanopores almost stayed the same was distinguished. Well-protected protein structures of GOD inside nanopore structures may lead to high activity of the enzyme, and may benefit the enzyme immobilization and even may achieve high sensitivity on enzyme biosensors. That is to say, nanopore structures were better adapted for the conformation retaining of enzymes than plane structures, and should be considered to build high sensitivity enzyme biosensors.

4. Conclusions

Unlike most previous experimental methods to study the effects of various functional nanostructures on the sensitivity of enzyme biosensors, this work built a set of comprehensive computing models of GOD/ZnO and GOD/gold hybrid systems for the mimic of glucose biosensors based on molecular dynamics simulation, where the underlying mechanisms among the enzyme conformations and biosensor nanostructures were demonstrated at the molecular scale. In the MD simulations, it was found that the different morphology and electric properties of ZnO and gold

substrates had different influences on the behaviors of GOD. On top of that, GOD with both 1-original and 2-x [90°] initial orientations had enormous conformation changes above both ZnO and gold plane surfaces, leading to the loss of their secondary structures, which could be one of the crucial reasons to enzyme inactivation or even low sensitivity in plane structure based biosensors cases. Meanwhile, the fact that GOD had the tendency to remain its own conformations inside of both ZnO and gold nanopores was distinguished. For the immobilization of GOD on enzyme biosensors, it is better to construct nanopore structures to make GOD stable. These results well tallied with the previously reported experimental results of ZnO and gold nanopore based biosensors having higher sensitivity than that of the plane structure based biosensors.

For the development of high sensitivity nanobiosensors, this study indicates that: 1) How to build biocompatible nanostructures to make enzyme stable should be considered first. Under the enzyme-activity guided strategies, developing well-regulated assembly processes to take the advantage of the high specific surface area inside the nanostructures is an important task to be fulfilled; 2) Molecular modeling and design of the biomolecule and nanostructure hybrid systems can help to develop more exquisite and robust enzyme biosensors.

Acknowledgements

This work was financially supported by the National Key Technology R&D Program of China (No. 2012BAI16B02), National Natural Science Foundation of

China (No. 60875078, 61501400) and Nature Science Foundation of Zhejiang Province of China under Grant Z1080300

References

1. Clark Jr, L. C.; Lyons, C. Electrode Systems for Continuous Monitoring in Cardiovascular Surgery. *Ann. NY. Acad. Sci.* **1962**, *102*, 29-45.

2. Vashist, S. K.; Zheng, D.; Al-Rubeaan, K.; Luong, J. H. T.; Sheu, F. S. Advances in Carbon Nanotube Based Electrochemical Sensors for Bioanalytical Applications. *Biotechnol. Adv.* **2011**, *29*, 169-188.

3. Liu, G.; Chen, H.; Peng, H.; Song, S.; Gao, J.; Lu, J.; Ding, M.; Li, L.; Ren, S.; Zou, Z.; Fan, C. A Carbon Nanotube-Based High-Sensitivity Electrochemical Immunosensor for Rapid and Portable Detection of Clenbuterol. *Biosens. Bioelectron.* **2011**, *28*, 308-313.

4. Tasca, F.; Harreither, W.; Ludwig, R.; Gooding, J. J.; Gorton, L. Cellobiose Dehydrogenase Aryl Diazonium Modified Single Walled Carbon Nanotubes: Enhanced Direct Electron Transfer through a Positively Charged Surface. *Anal. Chem.* **2011**, *83*, 3042-3049.

5. Wang, Y.; Liu, L.; Li, M.; Xu, S.; Gao, F. Multifunctional Carbon Nanotubes for Direct Electrochemistry of Glucose Oxidase and Glucose Bioassay. *Biosens. Bioelectron.* **2011**, *30*, 107-111.

6. Wooten, M.; Karra, S.; Zhang, M.; Gorski, W. On the Direct Electron Transfer, Sensing, and Enzyme Activity in the Glucose Oxidase/Carbon Nanotubes System. *Anal. Chem.* **2014**, *86*, 752-757.

7. Wu, P.; Shao, Q.; Hu, Y.; Jin, J.; Yin, Y.; Zhang, H.; Cai, C. Direct Electrochemistry of Glucose Oxidase Assembled on Graphene and Application to Glucose Detection. *Electrochim. Acta.* **2010**, *55*, 8606-8614.

8. Liang, B.; Fang, L.; Yang, G.; Hu, Y.; Guo, X.; Ye, X. Direct Electron Transfer Glucose Biosensor Based on Glucose Oxidase Self-Assembled on Electrochemically Reduced Carboxyl Graphene. *Biosens. Bioelectron.* **2013**, *43*, 131-136.

9. Liang, B.; Fang, L.; Hu, Y.; Yang, G.; Zhu, Q.; Ye, X. Fabrication and Application of Flexible Graphene Silk Composite Film Electrodes Decorated with Spiky Pt Nanospheres. *Nanoscale* **2014**, *6*, 4264-4274.

10. Song, Y.; Qu, K.; Zhao, C.; Ren, J.; Qu, X. Graphene Oxide: Intrinsic Peroxidase Catalytic Activity and Its Application to Glucose Detection. *Adv. Mater.* **2010**, *22*, 2206-2210.

11. Wang, Y.; Shao, Y.; Matson, D. W.; Li, J.; Lin, Y. Nitrogen-Doped Graphene and Its Application in Electrochemical Biosensing. *ACS Nano* **2010**, *4*, 1790-1798.

12. Wang, F.; Liu, X.; Lu, C. H.; Willner, I. Cysteine-Mediated Aggregation of Au Nanoparticles: The Development of a H_2O_2 Sensor and Oxidase-Based Biosensors. *ACS Nano* **2013**, *7*, 7278-7286.

13. Zeng, Q.; Cheng, J. S.; Liu, X. F.; Bai, H. T.; Jiang, J. H. Palladium Nanoparticle/Chitosan-Grafted Graphene Nanocomposites for Construction of a Glucose Biosensor. *Biosens. Bioelectron.* **2011**, *26*, 3456-3463.

14. Prakash, S.; Chakrabarty, T.; Singh, A. K.; Shahi, V. K. Polymer Thin Films Embedded with Metal Nanoparticles for Electrochemical Biosensors Applications. *Biosens. Bioelectron.* **2013**, *41*, 43-53.

15. Xu, J.; Shang, F.; Luong, J. H. T.; Razeeb, K. M.; Glennon, J. D. Direct Electrochemistry of Horseradish Peroxidase Immobilized on a Monolayer Modified Nanowire Array Electrode. *Biosens. Bioelectron.* **2010**, *25*, 1313-1318.

16. Li, L.; Huang, J.; Wang, T.; Zhang, H.; Liu, Y.; Li, J. An Excellent Enzyme Biosensor Based on Sb-Doped SnO_2 Nanowires. *Biosens. Bioelectron.* **2010**, *25*, 2436-2441.

17. Su, S.; He, Y.; Song, S.; Li, D.; Wang, L.; Fan, C.; Lee, S. T. A Silicon Nanowire-Based Electrochemical Glucose Biosensor with High Electrocatalytic Activity and Sensitivity. *Nanoscale* **2010**, *2*, 1704-1707.

18. Liu, Y.; Tuleouva, N.; Ramanculov, E.; Revzin, A. Aptamer-Based Electrochemical Biosensor for Interferon Gamma Detection. *Anal. Chem.* **2010**, *82*, 8131-8136.

19. Zhang, T.; Wang, W.; Zhang, D.; Zhang, X.; Ma, Y.; Zhou, Y.; Qi, L. Biotemplated Synthesis of Gold Nanoparticle–Bacteria Cellulose Nanofiber Nanocomposites and Their Application in Biosensing. *Adv. funct. mater.* **2010**, *20*, 1152-1160.

20. Dey, R. S.; Raj, C. R. Development of an Amperometric Cholesterol Biosensor Based on Graphene-Pt Nanoparticle Hybrid Material. *J. of Phys. Chem. C* **2010**, *114*, 21427-21433.

21. Jun, S. H.; Lee, J.; Kim, B. C.; Lee, J. E.; Joo, J.; Park, H.; Lee, J. H.; Lee, S. M.; Lee, D.; Kim, S.; et al. Highly Efficient Enzyme Immobilization and Stabilization within Meso-Structured Onion-Like Silica for Biodiesel Production. *Chem. Mater.* **2012**, *24*, 924-929.

22. Kim, J.; Grate, J. W.; Wang, P. Nanobiocatalysis and Its Potential Applications. *Trends. biotechnol.* **2008**, *26*, 639-646.

23. Pavlidis, I. V.; Vorhaben, T.; Tsoufis, T.; Rudolf, P.; Bornscheuer, U. T.; Gournis, D.; Stamatis, H. Development of Effective Nanobiocatalytic Systems Through the Immobilization of Hydrolases on Functionalized Carbon-Based Nanomaterials. *Bioresource. Technol.* **2012**, *115*, 164-171.

24. Gupta, R.; Chaudhury, N. K. Entrapment of Biomolecules in Sol-Gel Matrix for Applications in Biosensors: Problems and Future Prospects. *Biosens. Bioelectron.* **2007**, *22*, 2387-2399.

25. Qiu, H.; Lu, L.; Huang, X.; Zhang, Z.; Qu, Y. Immobilization of Horseradish Peroxidase on Nanoporous Copper and Its Potential Applications. *Bioresource. Technol.* **2010**, *101*, 9415-9420.

26. Mateo, C.; Palomo, J. M.; Fernandez-Lorente, G.; Guisan, J. M.; Fernandez-Lafuente, R. Improvement of Enzyme Activity, Stability and Selectivity via Immobilization Techniques. *Enzyme. Microb. Tech.* **2007**, *40*, 1451-1463.

27. Walcarius, A.; Minteer, S. D.; Wang, J.; Lin, Y.; Merkoci, A. Nanomaterials for bio-functionalized electrodes: recent trends. *J.Mater. Chem.B* **2013**, *1*, 4878-4908.

28. Sassolas, A.; Blum, L. J.; Leca-Bouvier, B. D. Immobilization Strategies to Develop Enzymatic Biosensors. *Biotechnol. Adv.* **2012**, *30*, 489-511.

29. Rubenwolf, S.; Kerzenmacher, S.; Zengerle, R.; Stetten, F. Strategies to Extend the Lifetime of Bioelectrochemical Enzyme Electrodes for Biosensing and Biofuel Cell Applications. *Appl. Microbiol. Biot.* **2010**, *89*, 1315-1322.

30. Nel, A.; Xia, T.; Mädler, L.; Li, N. Toxic Potential of Materials at the Nanolevel. *Science* **2006**, *311*, 622-627.

31. Chaniotakis, N. A. Enzyme Stabilization Strategies Based on Electrolytes and Polyelectrolytes for Biosensor Applications. *Anal. Bioanal. Chem.* **2004**, *378*, 89-95.

32. Carlsson, N.; Gustafsson, H.; Thörn, C.; Olsson, L.; Holmberg, K.; Åkerman, B. Enzymes Immobilized in Mesoporous Silica: A Physical-Chemical Perspective. *Adv. Colloid. Interfac.* **2014**, *205*, 339-360.

33. Schlipf, D. M.; Rankin, S. E.; Knutson, B. L. Pore-Size Dependent Protein Adsorption and Protection from Proteolytic Hydrolysis in Tailored Mesoporous Silica Particles. *ACS. appl. mater. inter.* **2013**, *5*, 10111-10117.

34. Xu, Z.; Duan, G.; Li, Y.; Liu, G.; Zhang, H.; Dai, Z.; Cai, W. CuO-ZnO Micro/Nanoporous Array-Film-Based Chemosensors: New Sensing Properties to H_2S. *Chem-Eur. J.* **2014**, *20*, 6040-6046.

35. Rahmanian, R.; Mozaffari, S. A.; Abedi, M. Disposable Urea Biosensor Based on Nanoporous ZnO Film Fabricated from Omissible Polymeric Substrate. *Mater. Sci. Eng.: C* **2015**, *57*, 387-396.

36. Wang, D.; Tan, Y. Electrodeposition of Enzymes-Integrated Mesoporous Composite Films by Interfacial Templating: A Paradigm for Electrochemical Biosensors. *Electrochim. Acta.* **2014**, *116*, 495-503.

37. Bai, S.; Sun, C.; Guo, T.; Luo, R.; Lin, Y.; Chen, A.; Sun, L.; Zhang, J. Low Temperature Electrochemical Deposition of Nanoporous ZnO Thin Films as Novel NO_2 Sensors. *Electrochim. Acta.* **2013**, *90*, 530-534.

38. Mozaffari, S. A.; Rahmanian, R.; Abedi, M.; Amoli, H. S. Urea Impedimetric Biosensor Based on Reactive RF Magnetron Sputtered Zinc Oxide Nanoporous Transducer. *Electrochim. Acta.* **2014**, *146*, 538-547.

39. Zhong, G.; Liu, A.; Chen, X.; Wang, K.; Lian, Z.; Liu, Q.; Chen, Y.; Du, M.; Lin, X. Electrochemical Biosensor Based on Nanoporous Gold Electrode for Detection of PML/RARα Fusion Gene. *Biosens. Bioelectron.* **2011**, *26*, 3812-3817.

40. Ahmadalinezhad, A.; Chen, A. High-Performance Electrochemical Biosensor for the Detection of Total Cholesterol. *Biosens. Bioelectron.* **2011**, *26*, 4508-4513.

41. Wu, C.; Liu, X.; Li, Y.; Du, X.; Wang, X.; Xu, P. Lipase-Nanoporous Gold Biocomposite Modified Electrode for Reliable Detection of Triglycerides. *Biosens. Bioelectron.* **2014**, *53*, 26-30.

42. Ahangar, L. E.; Mehrgardi, M. A. Nanoporous Gold Electrode as a Platform for the Construction of an Electrochemical DNA Hybridization Biosensor. *Biosens. Bioelectron.* **2012**, *38*, 252-257.

43. Hyeon, C.; Thirumalai, D. Capturing the Essence of Folding and Functions of Biomolecules Using Coarse-Grained Models. *Nat. Commun.* **2011**, *2*, 487.

44. Liu, K.; Ahmed, A.; Chung, S.; Sugikawa, K.; Wu, G.; Nie, Z.; Gordon, R.; Kumacheva, E. In Situ Plasmonic Counter for Polymerization of Chains of Gold Nanorods in Solution. *ACS Nano* **2013**, *7*, 5901-5910.

45. Radadia, A. D.; Stavis, C. J.; Carr, R.; Zeng, H.; King, W. P.; Carlisle, J. A.; Aksimentiev, A.; Hamers, R. J.; Bashir, R. Control of Nanoscale Environment to Improve Stability of Immobilized Proteins on Diamond Surfaces. *Adv. funct. mater.* **2011**, *21*, 1040-1050.

46. Rosenbaum, D. M.; Zhang, C.; Lyons, J. A.; Holl, R.; Aragao, D.; Arlow, D. H.; Rasmussen, S. G. F.; Choi, H.-J.; DeVree, B. T.; Sunahara, R. K.; et al. Structure and Function of an Irreversible Agonist-β_2 Adrenoceptor Complex. *Nature* **2011**, *469*, 236-240.

47. Artrith, N.; Kolpak, A. M. Understanding the Composition and Activity of Electrocatalytic Nanoalloys in Aqueous Solvents: A Combination of DFT and Accurate Neural Network Potentials. *Nano. Lett.* **2014**, *14*, 2670-2676.

48. Phadke, S.; Lee, J. Y.; West, J.; Peumans, P.; Salleo, A. Using Alignment and 2D Network Simulations to Study Charge Transport Through Doped ZnO Nanowire Thin Film Electrodes. *Adv. funct. mater.* **2011**, *21*, 4691-4697.

49. Yang, G.; Kang, Z.; Ye, X.; Wu, T.; Zhu, Q. Molecular Simulation of Flavin Adenine Dinucleotide Immobilized on Charged Single-Walled Carbon Nanotubes for Biosensor Applications. *Biomaterials* **2012**, *33*, 8757-8770.

50. Kane, R. S.; Stroock, A. D. Nanobiotechnology: Protein-Nanomaterial Interactions. *Biotechnol. Progr.* **2007**, *23*, 316-319.

51. Dai, Z.; Ju, H. Bioanalysis Based on Nanoporous Materials. *TrAC-Trend. Anal. Chem.* **2012**, *39*, 149-162.

52. Wu, C.; Sun, H. H.; Li, Y. F.; Liu, X. Y.; Du, X. Y.; Wang, X.; Xu, P. Biosensor Based on Glucose Oxidase-Nanoporous Gold Co-Catalysis for Glucose Detection. *Biosens. Bioelectron.* **2015**, *66*, 350-355.

53. Fang, B.; Zhang, C.; Wang, G.; Wang, M.; Ji, Y. A Glucose Oxidase Immobilization Platform for Glucose Biosensor Using ZnO Hollow Nanospheres. *Sensors. Actuat. B-Chem.* **2011**, *155*, 304-310.

54. Yang, Y. J.; He, Q.; Guo, L.; Zhang, H. Synthesis and Characterization of Nanoporous Gold Film for the Sensitive Detection of Glucose. *Sens. Lett.* **2013**, *11*, 650-655.

55. Hecht, H.; Kalisz, H.; Hendle, J.; Schmid, R.; Schomburg, D. Crystal Structure of Glucose Oxidase from Aspergillus niger Refined at 2· 3 Å Reslution. *J. Mol. Biol.* **1993**, *229*, 153-172.

56. MacKerrell, A.; Bashford, D.; Bellott, M.; Dunbrack, R.; Evanseck, J.; Field, M.; Fischer, S.; Gao, J.; Guo, H.; Ha, S. All-Atom Empirical Potential for Molecular Modeling and Dynamics Studies of Proteins. *J. Phys. Chem. B* **1998**, *102*, 3586-3616.

57. Zhao, X.; Johnson, J. K. Simulation of Adsorption of DNA on Carbon Nanotubes. *J. Am. Chem. Soc.* **2007**, *129*, 10438-10445.

58. Schäfer, I.; Lasko, G.; Do, T. A.; Pleiss, J.; Weber, U.; Schmauder, S. Peptide-Zinc Oxide Interaction: Finite Element Simulation Using Cohesive Zone Models Based on Molecular Dynamics Simulation. *Comp.Mater. Sci.* **2014**, *95*, 320-327.

59. Raymand, D.; van Duin, A. C. T.; Baudin, M.; Hermansson, K. A Reactive Force Field (ReaxFF) for Zinc Oxide. *Surf. Sci.* **2008**, *602*, 1020-1031.

60. Heinz, H.; Vaia, R. A.; Farmer, B. L.; Naik, R. R. Accurate Simulation of Surfaces and Interfaces of Face-Centered Cubic Metals Using 12-6 and 9-6 Lennard-Jones Potentials. *J. Phys. Chem. C* **2008**, *112*, 17281-17290.

61. Nawrocki, G.; Cieplak, M. Amino Acids and Proteins at ZnO-Water Interfaces in Molecular Dynamics Simulations. *Phys. Chem. Chem. Phys.* **2013**, *15*, 13628-13636.

62. Heinz, H.; Farmer, B. L.; Pandey, R. B.; Slocik, J. M.; Patnaik, S. S.; Pachter, R.; Naik, R. R. Nature of Molecular Interactions of Peptides with Gold, Palladium, and Pd-Au Bimetal Surfaces in Aqueous Solution. *J. Am. Chem. Soc.* **2009**, *131*, 9704-9714.

63. Humphrey, W.; Dalke, A.; Schulten, K. VMD: Visual Molecular Dynamics. *J. Mol. Graphics.* **1996**, *14*, 33-38.

64. Cheng, C. L.; Zhao, G. J. Steered Molecular Dynamics Simulation Study on Dynamic Delf-Assembly of Single-Stranded DNA with Double-Walled Carbon Nanotube and Graphene. *Nanoscale* **2012**, *4*, 2301-2305.

65. Kornherr, A.; French, S. A.; Sokol, A. A.; Catlow, C. R. A.; Hansal, S.; Hansal, W. E. G.; Besenhard, J. O.; Kronberger, H.; Nauer, G. E.; Zifferer, G. Interaction of Adsorbed Organosilanes with Polar Zinc Oxide Surfaces: A Molecular Dynamics Study Comparing Two Models for the Metal Oxide Surface. *Chem. Phys. Lett.* **2004**, *393*, 107-111.

66. Shen, J. W.; Wu, T.; Wang, Q.; Pan, H. H. Molecular Simulation of Protein Adsorption and Desorption on Hydroxyapatite Surfaces. *Biomaterials* **2008**, *29*, 513-532.

67. Tallury, S. S.; Pasquinelli, M. A. Molecular Dynamics Simulations of Flexible Polymer Chains Wrapping Single-Walled Carbon Nanotubes. *J. Phys. Chem. B.* **2010**, *114*, 4122-4129.

68. Chen, Q.; Kenausis, G. L.; Heller, A. Stability of Oxidases Immobilized in Silica Gels. *J. Am. Chem. Soc.* **1998**, *120*, 4582-4585.

69. Kong, T.; Chen, Y.; Ye, Y.; Zhang, K.; Wang, Z.; Wang, X. An Amperometric Glucose Biosensor Based on the Immobilization of Glucose Oxidase on the ZnO Nanotubes. *Sensor. Actuat. B-Chem.* **2009**, *138*, 344-350.

70. Xia, L.; Song, J.; Xu, R.; Liu, D. L,; Dong, B.; Xu, L.; Song, H.W. Zinc Oxide Inverse Opal Electrodes Modified by Glucose Oxidase for Electrochemical and Photoelectrochemical Biosensor. *Biosens. Bioelectron.* **2014**, *59*, 350-357.

71. Zhou, Y.; Wang, L.; Ye, Z. Z.; Zhao, M.G.; Cai, H.; Huang, J.Y. Mango Core Inner Shell Membrane Template-Directed Synthesis of Porous ZnO Films and Their Application for Enzymatic Glucose Biosensor. *Appl. Surf. Sci.* **2013**, *285*, 344-349.

72 Fatemi, H.; Khodadadi, A. A.; Anaraki Firooz, A.; Mortazavi, Y. Apple-Biomorphic Synthesis of Porous ZnO Nanostructures for Glucose Direct Electrochemical Biosensor. *Curr. Appl. Phys.* **2012**, *12*, 1033-1038.

73. Szamocki, R.; Velichko, A.; Mücklich, F.; Reculusa, S.; Ravaine, S.; Neugebauer, S.; Schuhmann, W.; Hempelmann, R.; Kuhn, A. Improved Enzyme Immobilization for Enhanced Bioelectrocatalytic Activity of Porous Electrodes. *Electrochem. Commun.* **2007**, *9*, 2121-2127.

74. Kashefi-Kheyrabadi, L.; Mehrgardi, M. A. Aptamer-Based Electrochemical Biosensor for Detection of Adenosine Triphosphate Using a Nanoporous Gold Platform. *Bioelectrochemistry* **2013**, *94*, 47-52.

75 Qiu, H. J.; Xue, L. Y.; Ji, G. L.; Zhou, G. P.; Huang, X. R.; Qu, Y. B.; Gao, P. J. Enzyme-Modified Nanoporous Gold-Based Electrochemical Biosensors. *Biosens. Bioelectron.* **2009**, *24*, 3014-3018.

76 Chen, L. Y.; Fujita, T.; Chen, M. W. Biofunctionalized Nanoporous Gold for Electrochemical Biosensors. *Electrochim. Acta.* **2012**, *67*, 1-5.

TOC Graphic

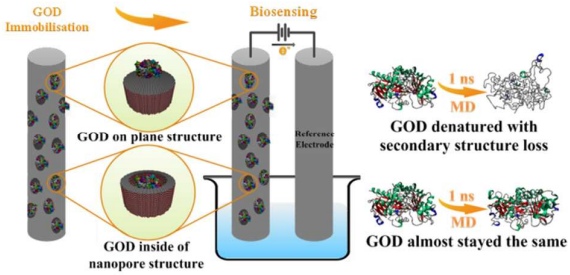
GOD
Immobilisation
Biosensing
GOD on plane structure
GOD inside of
nanopore structure
Reference
Electrode
1 ns
MD
GOD denatured with
secondary structure loss
1 ns
MD
GOD almost stayed the same